Electronic Supplementary Information

for

Design of One-Dimensional Organic Semiconductors with High Intrinsic Electron Mobilities: Lessons from Computation

Wenjun Xie,[a] *Weicong Huang,*[a] *Lingzhi Tu,*[a] *Hu Shi**[b] and *Hongguang Liu**[a,c]

[a] College of Chemistry and Materials Science, Jinan University, 601 Huang-Pu Avenue West, Guangzhou 510632, China. E-mail: hongguang_liu@jnu.edu.cn

[b] School of Chemistry and Chemical Engineering, Shanxi University, Taiyuan 030006, China. E-mail: hshi@sxu.edu.cn

[c] Guangdong Provincial Key Laboratory of Functional Supramolecular Coordination Materials and Applications, Jinan University, 601 Huang-Pu Avenue West, Guangzhou 510632, China.

Contents

1. Computational details

1.1 Quantum mechanical calculation

1.1.1 Binding energy calculation

All quantum mechanical calculations were performed using the Gaussian 09 package.[1] The structures of molecules if not specified were optimized by the density functional theory at the M06-2X/6-31+g(d) level.[2] Among the tested hybrid meta exchange-correlation functionals, M06-2X was proven to offer the best results for the combination of main-group thermochemistry, kinetics, and noncovalent interactions.[3] "Integral=ultrafine" option was employed to minimize the integration grid errors that may result from using an inadequate grid in the current M06 suite of functionals.[4] All structure optimizations have no additional constraints. Frequency calculations were performed at the same level of theory to identify all of the stationary points as minima (zero imaginary frequencies). All computed binding energies were corrected for basis-set superposition error (BSSE) by using the counterpoise method of Boys and Bernardi.[5]

1.1.2 Transfer integral calculation

The transfer integral t for electron transport was computed using the Koopmans' theorem,[6] depending on the one-electron approximation:

$$t = \frac{E_{L+1} - E_L}{2}$$

where E_L and E_{L+1} are the energies of the LUMO and LUMO+1 respectively in the closed-shell configuration of the neutral state of a dimer. Note that t computed by this method agrees well with the absolute t computed by the direct quantum mechanical method, which is consistent with that reported by Valeev et al.[7] for cofacial dimers composed of identical monomers.

1.1.3 Internal reorganization energy calculation

The internal electron reorganization energy λ was calculated via the Nelsen's four-point approach.[8] It is described as the vertical ionization of a neutral molecule followed

by geometric relaxation and then the vertical neutralization of a charged molecule followed by geometric relaxation:

$$\lambda = E\text{–}(Q0) - E\text{–}(Q\text{–}) + E0(Q\text{–}) - E0(Q0)$$

where E is energy, Q is geometry, and the subscripts 0 and – denote neutral and anionic states, respectively. The energies of neutral and anionic monomers were obtained at the B3LYP/6-31g(d,p) level,[9] because this level of theory has been shown to afford λ values that agree with experimental values extracted from the gas-phase photoelectron spectra.[10] Although in ref 10 the normal-mode method instead of the four-point method was used to compute λ, these two methods are known to give consistent results for this parameter[11] at the B3LYP/6-31g(d,p) level. λ for PyDI, PDI and NDI is computed to be 0.22, 0.26 and 0.33 eV, respectively. λ for **7'** and **8a'** is 0.33 and 0.27 eV, respectively.

1.1.4 Mobility calculation

At room temperature, charge transport within organic semiconductor can be described as a hopping mechanism. The charge transfer rate k_{CT} between two neighboring molecules can be calculated using the semiclassical Marcus theory:[12]

$$k_{CT} = \frac{4\pi^2}{h}\frac{1}{\sqrt{4\pi\lambda k_B T}}t^2 \exp\left(-\frac{\lambda}{4k_B T}\right)$$

The electron mobility can be calculated by applying the Einstein-Smoluchowski relation:[13]

$$\mu = e L^2 k_{CT}/2k_B T$$

where e is the electronic charge, L is the transport distance (approximated by the molecular center-to-center distance of a dimer), k_B is the Boltzmann constant, and T is the temperature.

1.2 Molecular mechanics simulation

The all-atom classical molecular dynamics (MD) simulations were carried out using the Amber18 package.[14] Force field parameters for solute and solvent C_6H_6 were generated at the B3LYP/6-31+g(d) optimized geometry using the Gaussian 09 package, because this level of theory is widely used for force field constructions in organic semiconductors.[15] Atomic structure and force field parameters for solvent $CHCl_3$ were

borrowed from the solvent model already implemented in the Amber18 package. Energy minimizations were performed using a combination of steepest descent and conjugate gradient algorithms. The time step used in all simulations was 2 fs. MD simulations have been performed under periodic boundary conditions and the coordinates of all atoms in the simulation box were saved every 2 ps. The minimum distance between any atom of the aggregate and the periodic box edge was set to be 10 Å. All bonds involving hydrogens were fixed with the SHAKE algorithm.[16] The initial velocities of all atoms were chosen randomly according to a Maxwell-Boltzmann distribution. MD simulations were performed in the NPT ensemble. The temperature was kept constant using a Langevin thermostat[17] at 300 K with a collision frequency of 2 ps^{-1}. The pressure was controlled by a Berendsen barostat[18] at 1 bar with a relaxation time of 1 ps. The electrostatic term was computed using the Particle-Mesh-Ewald summation method[19] and the cutoff algorithm was applied for non-bonded interactions with a radius of 8 Å. The systems were initially heated up for 500 ps in the NVT ensemble with restraints for atomic positions (force constant of 20 kcal/mol/$Å^2$) and then equilibrated in the NPT ensemble for 500 ps with no restraint at 300 K. The duration of each MD trajectory was 100 ns. The final MD-simulated atomic structures of 1D helical aggregates were rendered by the Visual Molecular Dynamics (VMD) software[20] based on the files exported from Amber18. To study the self-organization processes of **7'** (Fig.5a) and **8a'** (Fig.5b), solute molecules prior to MD simulations were randomly distributed in a cubic $CHCl_3$ box (80 Å×80 Å×80 Å, solute/solvent molar ratio=1:120) by Gromacs 5.1.5.[21]

2. Fig.S1

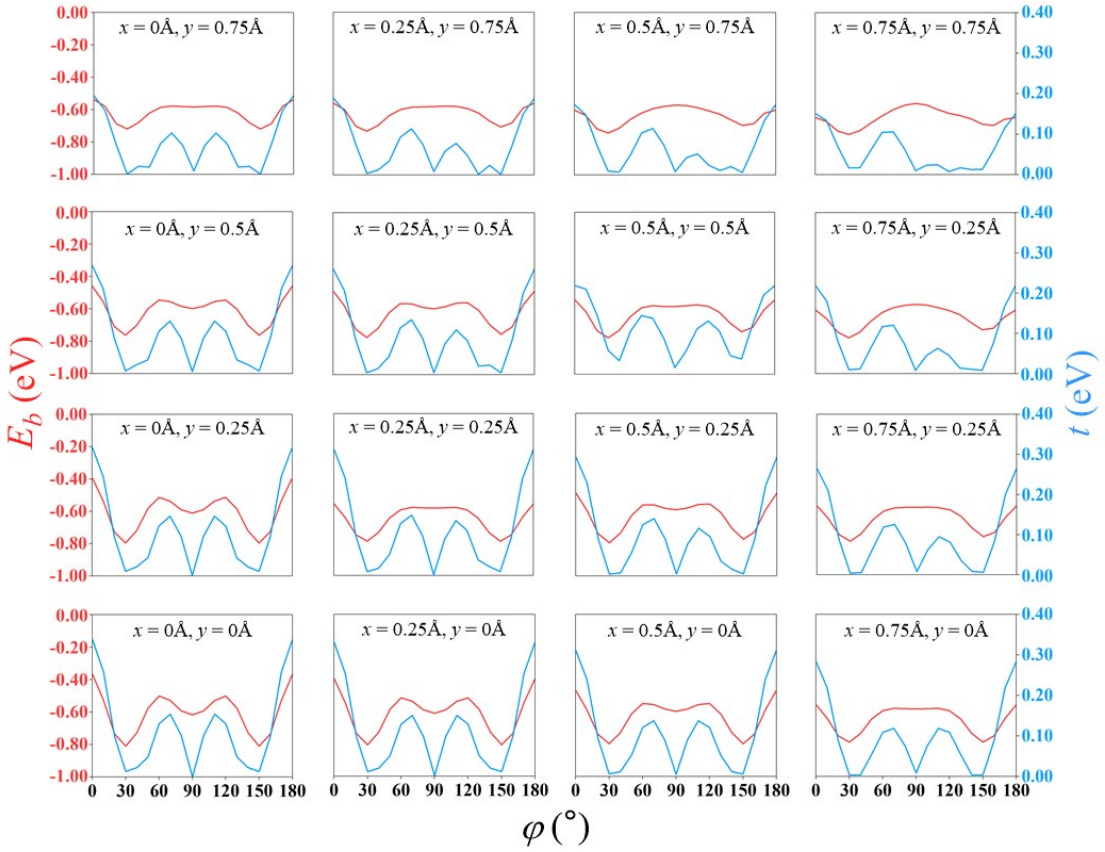

Fig.S1 Binding energy E_b and transfer integral t as a function of the twist angle φ for sandwiched stacks of PDI with lateral displacements. The intermolecular separation is fixed at 3.6 Å.

3. Fig.S2

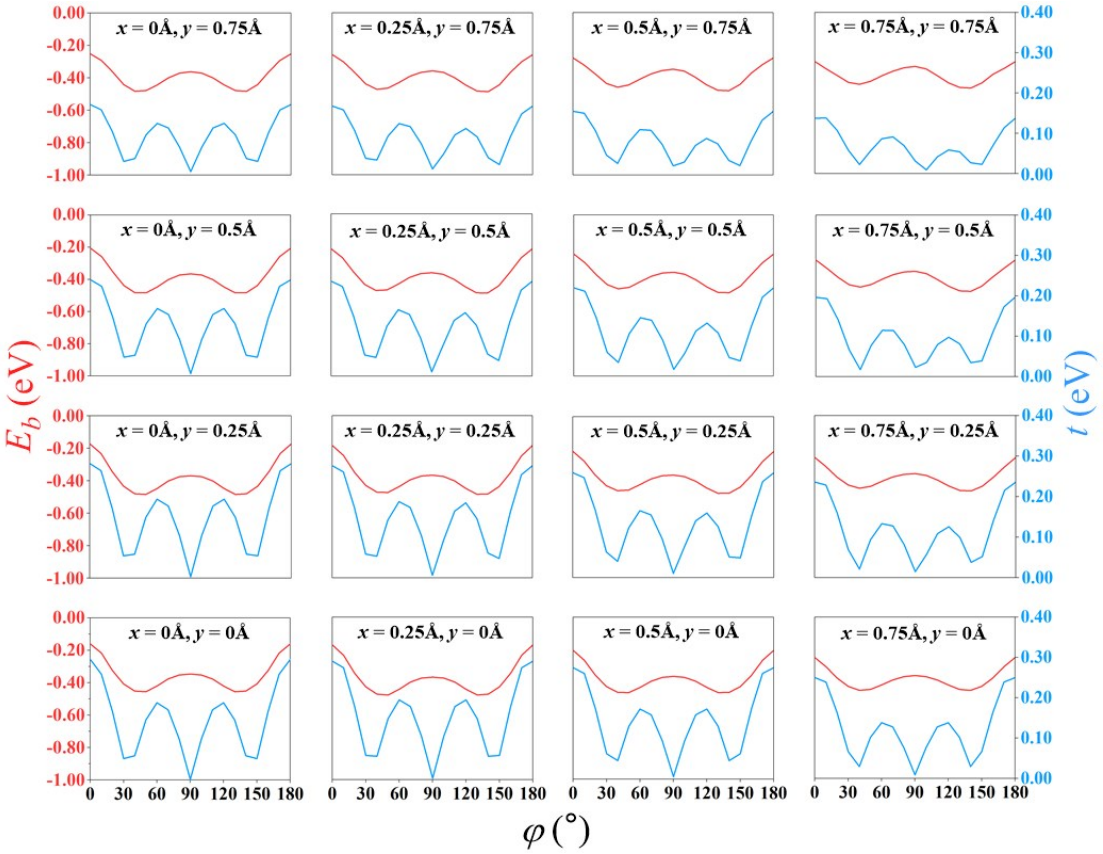

Fig.S2 Binding energy E_b and transfer integral t as a function of the twist angle φ for sandwiched stacks of NDI with lateral displacements. The intermolecular separation is fixed at 3.6 Å.

4. Fig.S3

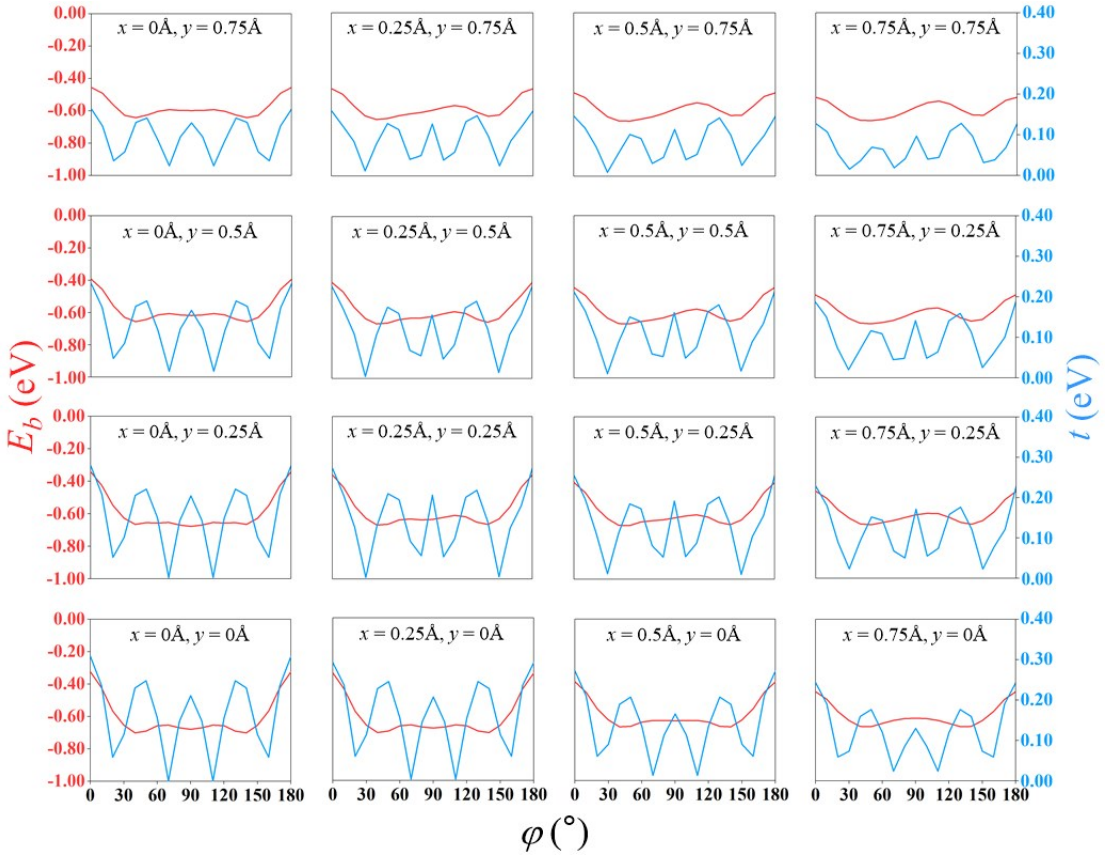

Fig.S3 Binding energy E_b and transfer integral t as a function of the twist angle φ for sandwiched stacks of PyDI with lateral displacements. The intermolecular separation is fixed at 3.6 Å.

5. Fig.S4

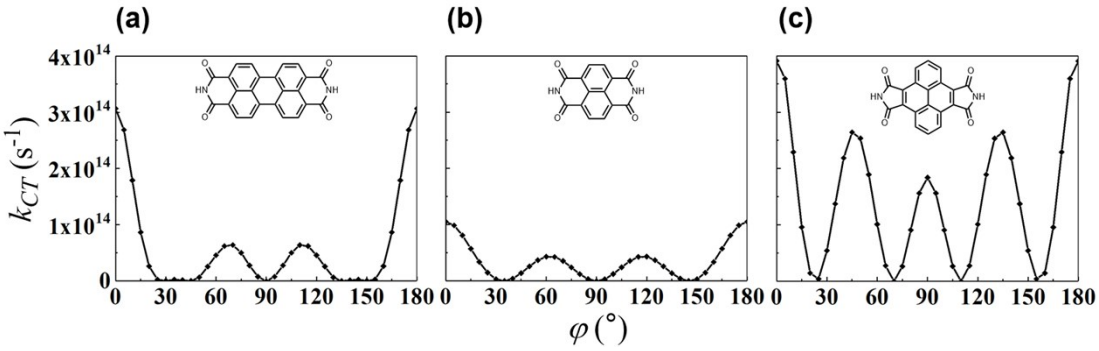

Fig.S4 Charge transfer rate k_{CT} as a function of the twist angle φ for sandwiched stacks of (a) PDI, (b) NDI and (c) PyDI.

6. Table.S1 Twist angles for tightly-bound dimers reported in Fig.2b

x /Å	y /Å	φ (°)	E_b (eV)
0.00	0.00	40	-0.701
0.25	0.00	40	-0.706
0.50	0.00	40	-0.667
0.75	0.00	50	-0.664
1.00	0.00	50	-0.661
1.25	0.00	50	-0.653
1.50	0.00	50	-0.640
1.75	0.00	50	-0.621
2.00	0.00	40	-0.609
0.00	0.25	40	-0.665
0.25	0.25	40	-0.668
0.50	0.25	40	-0.668
0.75	0.25	50	-0.660
1.00	0.25	60	-0.667
1.25	0.25	50	-0.663
1.50	0.25	50	-0.660
1.75	0.25	60	-0.654
2.00	0.25	60	-0.637
0.00	0.50	40	-0.656
0.25	0.50	40	-0.662
0.50	0.50	50	-0.666
0.75	0.50	50	-0.666
1.00	0.50	60	-0.654
1.25	0.50	60	-0.659
1.50	0.50	60	-0.659
1.75	0.50	60	-0.651
2.00	0.50	60	-0.634
0.00	0.75	40	-0.642
0.25	0.75	40	-0.653
0.50	0.75	50	-0.662
0.75	0.75	50	-0.662
1.00	0.75	120	-0.651
1.25	0.75	60	-0.638
1.50	0.75	60	-0.640
1.75	0.75	60	-0.635
2.00	0.75	60	-0.618
0.00	1.00	40	-0.624
0.25	1.00	40	-0.641
0.50	1.00	50	-0.655
0.75	1.00	50	-0.658
1.00	1.00	40	-0.653
1.25	1.00	40	-0.636
1.50	1.00	30	-0.622
1.75	1.00	30	-0.605
2.00	1.00	130	-0.590
0.00	1.25	40	-0.605
0.25	1.25	50	-0.626
0.50	1.25	50	-0.647
0.75	1.25	40	-0.654
1.00	1.25	50	-0.651
1.25	1.25	50	-0.637
1.50	1.25	40	-0.619
1.75	1.25	40	-0.601
2.00	1.25	40	-0.579
0.00	1.50	40	-0.584
0.25	1.50	50	-0.615
0.50	1.50	50	-0.637
0.75	1.50	50	-0.643
1.00	1.50	40	-0.642
1.25	1.50	40	-0.632
1.50	1.50	40	-0.613
1.75	1.50	40	0.590
2.00	1.50	30	-0.570
0.00	1.75	60	-0.577
0.25	1.75	50	-0.601
0.50	1.75	50	-0.621
0.75	1.75	50	-0.628
1.00	1.75	40	-0.621
1.25	1.75	40	-0.614
1.50	1.75	40	-0.600
1.75	1.75	40	-0.580
2.00	1.75	40	-0.560
0.00	2.00	60	-0.569
0.25	2.00	60	-0.583
0.50	2.00	50	-0.598
0.75	2.00	50	-0.603
1.00	2.00	50	-0.598
1.25	2.00	40	-0.585
1.50	2.00	40	-0.575
1.75	2.00	40	-0.560
2.00	2.00	40	-0.542

7. Fig.S5

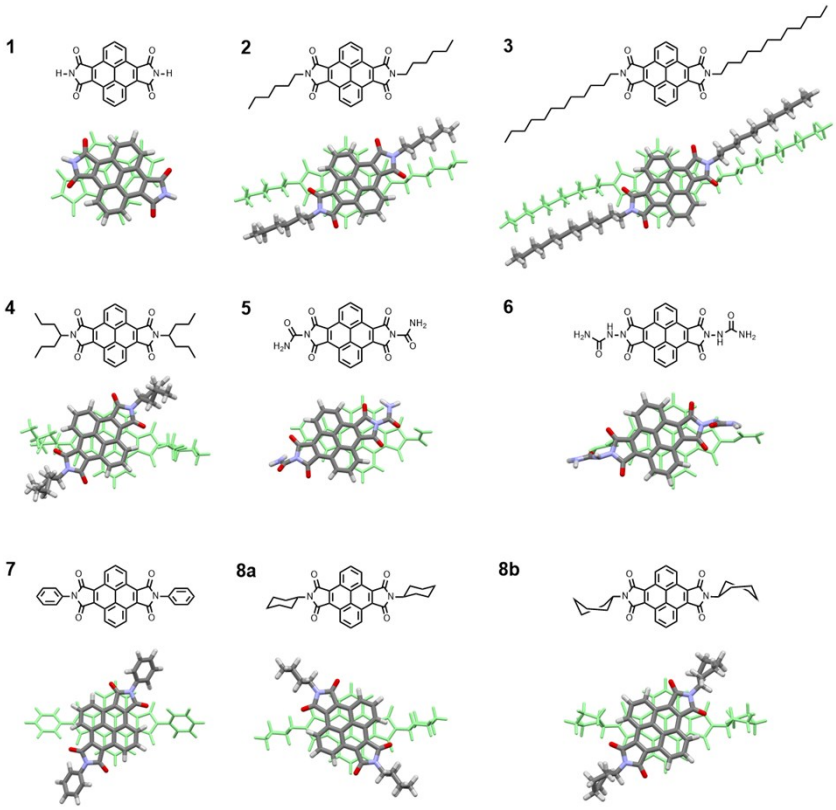

Fig.S5 Dimer structures in Fig.3.

8. Fig.S6

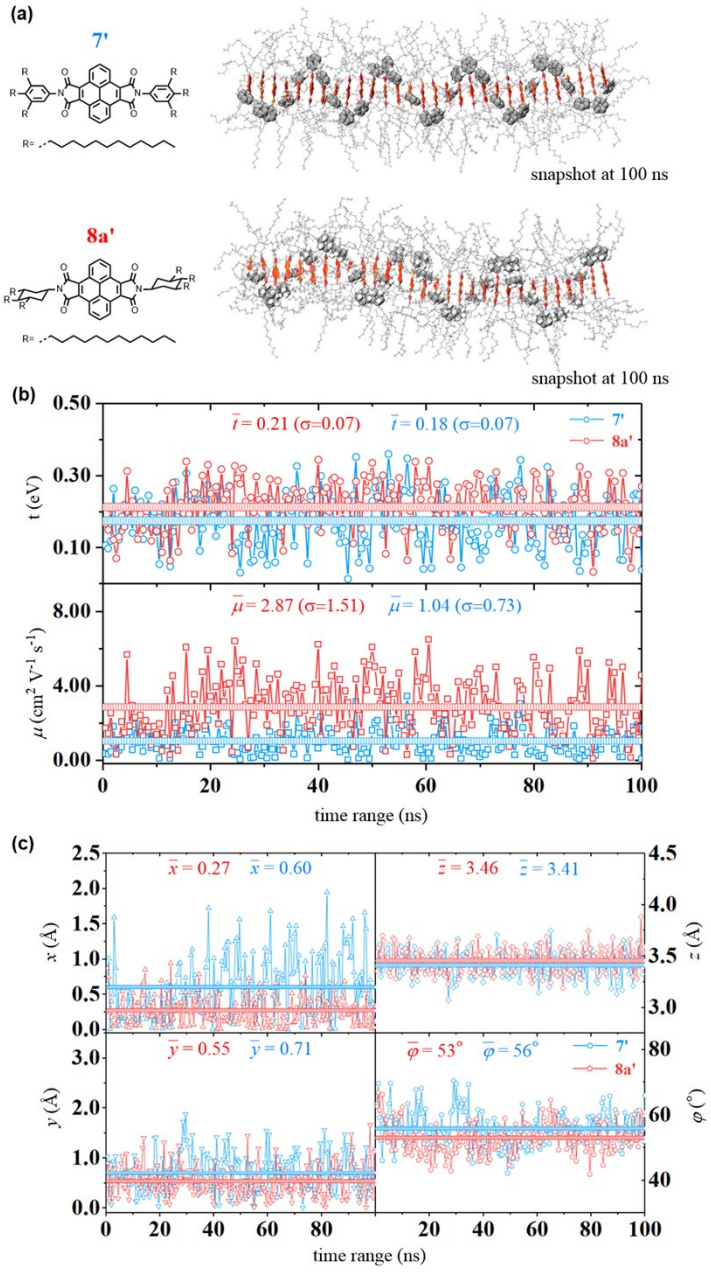

Fig.S6 (a) Final MD-simulated atomic structures of the 1D helical aggregates of **7'** and **8a'** in C_6H_6 at 300 K. For clarity, solvent C_6H_6 are omitted. The PyDI cores are highlighted in red and one-side of ring aggregators are zoomed in to show the helicity; (b) computed t and electron mobilities μ for **7'** and **8a'** based on snapshots of the inner-most dimer of each complete aggregate saved every 0.5 ns in a 100 ns MD simulation. σ in the parenthesis is the standard deviation; (c) x, y, z displacements and twist angles φ extracted from the same set of snapshots of (b)

9. Fig.S7

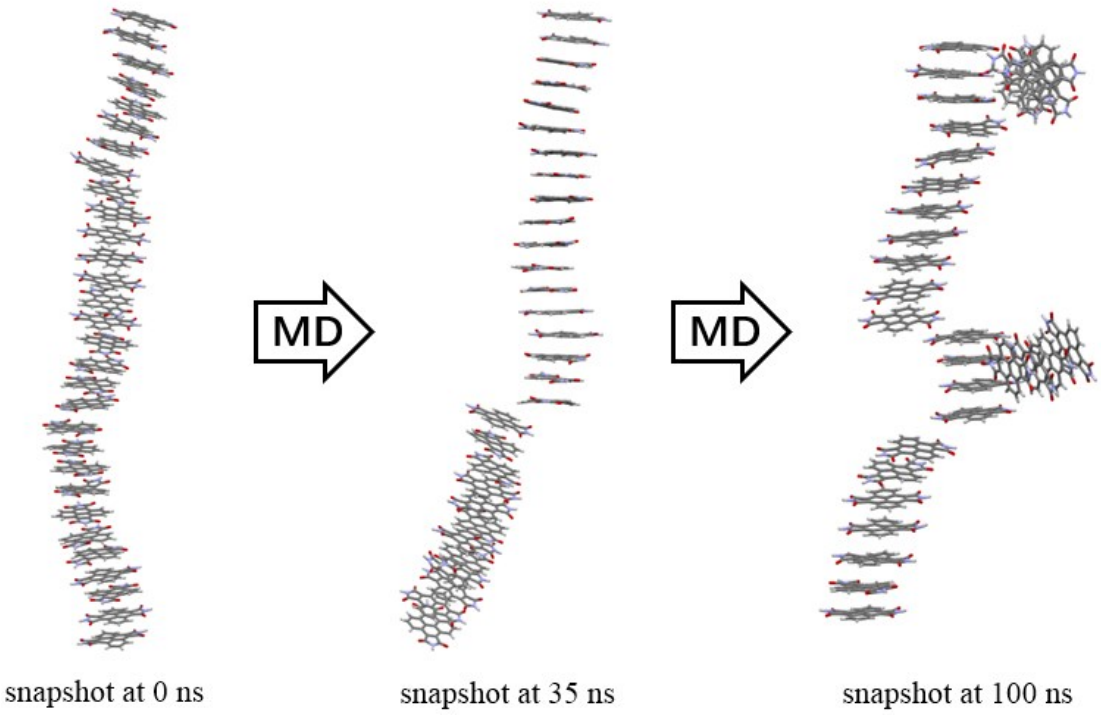

Fig.S7 MD-simulated structure evolution of the 1D helical aggregate of the unsubstituted PyDI in $CHCl_3$ at 300 K. For clarity, solvent $CHCl_3$ are omitted.

10. Reference

1 M. J. Frisch, G.W. Trucks, H. B. Schlegel, G. E. Scuseria, M. A. Robb, J. R. Cheeseman, G. Scalmani, V. Barone, B. Mennucci, G. A. Petersson, H. Nakatsuji, M. Caricato, X. Li, H. P. Hratchian, A. F. Izmaylov, J. Bloino, G. Zheng, J. L. Sonnenberg, M. Hada, M. Ehara, K. Toyota, R. Fukuda, J. Hasegawa, M. Ishida, T. Nakajima, Y. Honda, O. Kitao, H. Nakai, T. Vreven, J. A. Montgomery, Jr., J. E. Peralta, F. Ogliaro, M. Bearpark, J. J. Heyd, E. Brothers, K. N. Kudin, V. N. Staroverov, R. Kobayashi, J. Normand, K. Raghavachari, A. Rendell, J. C. Burant, S. S. Iyengar, J. Tomasi, M. Cossi, N. Rega, J. M. Millam, M. Klene, J. E. Knox, J. B. Cross, V. Bakken, C. Adamo, J. Jaramillo, R. Gomperts, R. E. Stratmann, O. Yazyev, A. J. Austin, R. Cammi, C. Pomelli, J. W. Ochterski, R. L. Martin, K. Morokuma, V. G. Zakrzewski, G. A. Voth, P. Salvador, J. J. Dannenberg, S. Dapprich, A. D. Daniels, O. Farkas, J. B. Foresman, J. V. Ortiz, J. Cioslowski, D. J. Fox, Gaussian 09, Revision E.01 Gaussian, Inc., Wallingford CT, 2009.

2 Y. Zhao and D. G. Truhlar, *Acc. Chem. Res.*, 2008, **41**, 157-167.

3 Y. Zhao and D. G. Truhlar, *Theor. Chem. Acc.*, 2008, **120**, 215-241.

4 S. E. Wheeler and K. N. Houk, *J. Chem. Theory Comput.*, 2010, **6**, 395-404.

5 S. F. Boys and F. Bernardi, *Mol. Phys.*, 2002, **100**, 65-73.

6 T. Koopmans, *Physica*, 1934, **1**, 104-113.

7 E. F. Valeev, V. Coropceanu, D. A. da Silva Filho, S. Salman and J. Brédas, *J. Am. Chem. Soc.*, 2006, **128**, 9882-9886.

8 (*a*) S. F. Nelsen, S. C. Blackstock and Y. Kim, *J. Am. Chem. Soc.*, 1987, **109**, 677-682; (*b*) S. F. Nelsen and M. J. R. Yunta, *J. Phys. Org. Chem.*, 1994, **7**, 55-62.

9 (*a*) C. Lee, W. Yang and R. G. Parr, *Phys. Rev. B*, 1988, **37**, 785-789; (*b*) A. D. Becke, *J. Chem. Phys.*, 1993, **98**, 5648-5652.

10 N. E. Gruhn, D. A. da Silva Filho, T. G. Bill, M. Malagoli, V. Coropceanu, A. Kahn and J. Brédas, *J. Am. Chem. Soc.*, 2002, **124**, 7918-7919..

11 (*a*) J. Brédas, D. Beljonne, V. Coropceanu and J. Cornil, *Chem. Rev.*, 2004, **104**, 4971-5004; (*b*) M. C. R. Delgado, K. R. Pigg, D. A. da Silva Filho, N. E. Gruhn, Y. Sakamoto, T. Suzuki, R. M. Osuna, J. Casado, V. Hernández, J. T. L. Navarrete, N. G. Martinelli, J. Cornil, R. S. Sánchez-Carrera, V. Coropceanu and J. Brédas, *J. Am. Chem. Soc.*, 2009, **131**, 1502-1512.

12 (*a*) R. A. Marcus, *Rev. Mod. Phys.*, 1993, **65**, 599-610; (*b*) P. F. Barbara, T. J. Meyer and M. A. Ratner, *J. Phys. Chem.*, 1996, **100**, 13148-13168; (*c*) J. Cornil, J. Brédas, J. Zaumseil and H. Sirringhaus, *Adv. Mater.*, 2007, **19**, 1791-1799.

13 P. Atkins, J. De Paula and R. Friedman, *Physical Chemistry: Quanta, Matter, and Change*, Oxford University Press, USA, 2013.

14 D.A. Case, I.Y. Ben-Shalom, S.R. Brozell, D.S. Cerutti, T.E. Cheatham, III, V.W.D. Cruzeiro, T.A. Darden, R.E. Duke, D. Ghoreishi, M.K. Gilson, H. Gohlke, A.W. Goetz, D. Greene, R Harris, N. Homeyer, S. Izadi, A. Kovalenko, T. Kurtzman, T.S. Lee, S. LeGrand, P. Li, C. Lin, J. Liu, T. Luchko, R. Luo, D.J. Mermelstein, K.M. Merz, Y. Miao, G. Monard, C. Nguyen, H. Nguyen, I. Omelyan, A. Onufriev, F. Pan, R. Qi, D.R. Roe, A. Roitberg, C. Sagui, S. Schott-Verdugo, J. Shen, C.L. Simmerling, J. Smith, R. Salomon-Ferrer, J. Swails, R.C. Walker, J. Wang, H. Wei, R.M. Wolf, X. Wu, L. Xiao, D.M. York and P.A. Kollman, AMBER18, University of California, San Francisco, 2018.

15 (*a*) J. Torras, D. Zanuy, D. Aradilla and C. Alemán, *Phys. Chem. Chem. Phys.*, 2016, **18**, 24610-24619; (*b*) S. Inoue, S. Shinamura, Y. Sadamitsu, S. Arai, S. Horiuchi, M. Yoneya, K. Takimiya and T. Hasegawa, *Chem. Mater.*, 2018, **30**, 5050-5060; (*c*) M. Yoneya, *J. Phys. Chem. C*, 2018, **122**, 22225-22231.

16 J. P. Ryckaert, G. Ciccotti and H. J. Berendsen, *J. computat. phys.*, 1977, **23**, 327-341.

17 R. J. Loncharich, B. R. Brooks and R. W. Pastor, *Biopolymers*, 1992, **32**, 523-535.

18 H. J. C. Berendsen, J. P. M. Postma, W. F. van Gunsteren, A. DiNola and J. R. Haak, *J. Chem. Phys.*, 1984, **81**, 3684-3690.

19 T. Darden, D. York and L. Pedersen, *J. Chem. Phys.*, 1993, **98**, 10089-10092.

20 W. Humphrey, A. Dalke and K. Schulten, *J. Mol. Graph.*, 1996, **14**, 33-38.

21 M. J. Abraham, T. Murtola, R. Schulz, S. Páll, J. C. Smith, B. Hess and E. Lindahl, *SoftwareX*, 2015, **1-2**, 19-25.